

SCIENTIFIC REPORTS



OPEN

Validated prediction of pro-invasive growth factors using a transcriptome-wide invasion signature derived from a complex 3D invasion assay

Received: 22 December 2014

Accepted: 03 June 2015

Published: 05 August 2015

Bettina Oehrle¹, Gerald Burgstaller¹, Martin Irmeler², Stefan Dehmel¹, Jessica Grün¹, Tiffany Hwang¹, Susanne Krauss-Etschmann¹, Johannes Beckers^{2,3}, Silke Meiners¹ & Oliver Eickelberg¹

The invasion of activated fibroblasts represents a key pathomechanism in fibrotic diseases, carcinogenesis and metastasis. Invading fibroblasts contribute to fibrotic extracellular matrix (ECM) formation and the initiation, progression, or resistance of cancer. To construct transcriptome-wide signatures of fibroblast invasion, we used a multiplex phenotypic 3D invasion assay using lung fibroblasts. Microarray-based gene expression profiles of invading and non-invading fibroblasts demonstrated that 1,049 genes were differentially regulated (>1.5-fold). Unbiased pathway analysis (Ingenuity) identified significant enrichment for the functional clusters 'invasion of cells', 'idiopathic pulmonary fibrosis', and 'metastasis'. Matrix metalloproteinase 13 (MMP13), transforming growth factor (TGF)- β 1, Caveolin (Cav) 1, Phosphatase and Tensin Homolog (Pten), and secreted frizzled-related protein (Sfrp) 1 were among the highest regulated genes, confirmed by qRT-PCR and Western Blotting. We next performed *in silico* analysis (Ingenuity Pathway Analysis) to predict mediators that induced fibroblast invasion. Of these, TGF β 1, epidermal growth factor (EGF), fibroblast growth factor (FGF) 2, and platelet-derived growth factor (PDGF)-BB were tested in our 3D invasion assay and found to significantly induce invasion, thus validating the transcriptome profile. Accordingly, our transcriptomic invasion signature describes the invading fibroblast phenotype in unprecedented detail and provides a tool for future functional studies of cell invasion and therapeutic modulation thereof using complex phenotypic assays.

Fibroblast invasion through interstitial tissue is one substantial step in the dynamic process of tissue remodelling and repair, a process that also plays a pivotal role in fibrogenesis¹, carcinogenesis, and metastasis^{2,3}. Cell migration through the three-dimensional (3D) architecture of most tissues, in particular the lung, requires an invading phenotype that enables fibroblasts to penetrate the extracellular matrix (ECM) and cross the basal membrane. This migratory program is an inherent feature of many cells, such as fibroblasts or leukocytes, yet it can also be specifically increased during inflammation or tissue

¹Comprehensive Pneumology Center, University Hospital of the Ludwig-Maximilians-University Munich and Helmholtz Zentrum München, Member of the German Center for Lung Research, 81377 Munich, Germany.

²Institute of Experimental Genetics, Helmholtz Zentrum München, German Research Center for Environmental Health (GmbH), 85764 Neuherberg, Germany. ³Technical University Munich, Chair of Experimental Genetics, 85350 Freising-Weihenstephan, Germany. Correspondence and requests for materials should be addressed to O.E.

(email: oliver.eickelberg@helmholtz-muenchen.de)

wounding⁴. Importantly, the mode of interstitial migration differs between various cell types: leukocytes are mainly found to display an integrin-independent amoeboid mode of migration, while most cancer cells and fibroblasts display mesenchymal movements⁵.

In tissue fibrosis, such as idiopathic pulmonary fibrosis (IPF), areas of activated fibroblasts, are believed to represent the site of increased production, secretion, and deposition of ECM^{6,7}. In the lung, α -smooth muscle actin (α SMA)-positive fibroblasts originate from the sub-pleural region and form a fibroblastic reticular structure into the interstitium⁸. It is widely assumed that this process requires an invading fibroblast phenotype⁹. During injury, repair, and fibrosis, a plethora of soluble mediators are released by different cell types, which activate and attract resident fibroblasts and/or induce transformation of epithelial or pleural mesothelial cells (PMC) into mesenchymal-like cells^{10–13}. Such aberrantly activated mesenchymal cells exhibit an exceptional plasticity with respect to proliferation, apoptosis, ECM deposition, activation, and tissue invasion¹¹. In agreement with this concept, an increased collagen-invading capacity of human lung fibroblasts derived from IPF patients has recently been reported in 2D assays¹⁴. Furthermore, keloid fibroblasts are suggested to exhibit a highly invasive character, inducing infiltration of these fibroblasts into surrounding healthy skin tissue¹⁵. Enhanced fibroblast invasion, however, does play a decisive role in carcinogenesis and metastasis, as the tumour microenvironment is increasingly recognized as a major feature of tumour progression³. Here, the crosstalk between cancer cells and cells of the neoplastic stroma are important factors for invasive tumour growth and metastasis^{16,17}. In particular, cancer associated fibroblasts (CAF) have been reported to represent key determinants in cancer progression². Studies using squamous cell carcinoma (SCC) cells and stromal fibroblasts revealed that force- and protease-mediated matrix remodelling by the fibroblast is required for collective invasion of the SCC cells¹⁸, indicating that invading fibroblasts are able to direct carcinoma cells through stromal tissue.

In the current study, we hypothesized that pathway analysis of the transcriptome-wide signature of invading lung fibroblasts by comparative microarray analyses, using a collagen-based invasion assay previously established in our lab¹⁹, will identify pro-invasive growth factors with relevance to disease. To this end, we generated a specific fibroblast invasion signature, followed by functional validation of *in silico*-predicted upstream regulators of fibroblast invasion; namely transforming growth factor (TGF) β 1, epidermal growth factor (EGF), fibroblast growth factor 2 (FGF2), and platelet-derived growth factor (PDGF)-BB. Prospectively, this validated fibroblast invasion signature will enable the identification of yet unknown invasion-relevant molecular networks and underlying mechanisms thereof. Thus, this invasion signature advances the understanding of an activated invasive fibroblast phenotype in particular for fibrotic and metastatic pathologies.

Results Section

Deciphering a transcriptomic signature for invading fibroblasts. In order to systematically identify the molecular signature of invading fibroblasts we applied a whole transcriptome analysis (Affymetrix Mouse Gene 1.0 ST array), using our recently established 3D invasion assay¹⁹. A subpopulation of murine MLg 2908 (MLg) lung fibroblasts spontaneously invaded a 3D collagen matrix when plated on top of it¹⁹. Separation of invading from non-invading MLg fibroblasts was carried out 72 or 96 hours after plating. RNA isolation and subsequent whole transcriptome analysis provided gene expression profiles of invading and non-invading fibroblasts. Transcripts with a false discovery rate <10% were considered as being statistically significant regulated and were used for subsequent analyses. After 72 hours of invasion, 1,086 targets with expression ratios greater than 1.5-fold and 163 targets regulated greater than 2-fold were identified in the invading fraction as compared to the non-invading fraction. In fibroblasts that invaded the matrix for 96 hours, an altered regulation of 1,049 probes with expression ratios greater than 1.5-fold and 182 greater than 2-fold were identified (Fig. 1A). Hierarchical clustering of the different fractions is depicted in Fig. 1B. Heatmaps of up- and down-regulated target genes (>2-fold) in the invading fractions at 72 hours and 96 hours validate the reproducibility of our replicate analyses (Fig. 2A and Fig. 2B). The whole array data have been submitted to GEO (GSE55322).

Predictive *in silico* cluster analysis and validation of the gene expression profile of fibroblast invasion. The gene expression profiles of the invading fibroblasts at 72 hours and 96 hours (>1.5-fold) greatly overlapped: among the differentially regulated genes in the invading subtype at 72 and 96 hours, 621 genes overlapped in total: 166 in the up- and 455 in the down-regulated group (Fig. 3A). Of note, there were more than twice as many overlapping down-regulated genes than overlapping up-regulated genes. This comparative approach allowed us to enrich for those targets that are commonly regulated after 72 and 96 hours of invasion and to define the invasion signature of fibroblasts. Enrichment analyses using IPA's 'disease and function' ontology revealed that 'invasion of cells', 'idiopathic pulmonary fibrosis (IPF)', and 'metastasis' ranked as the top three most significantly over-represented 'disease processes' and 'biological functions' within the invasion signature (Fig. 3B). In agreement with the well-known role of TGF β 1 in invasion and fibrosis, TGF β 1 associated with all three key networks of invasion (Fig. 3C). These data clearly corroborate our experimental approach. In order to further validate the profiling approach used, several known invasion-promoting genes were chosen for confirmative expression analysis by qRT-PCR. These targets included matrix metalloprotease 13 (MMP13)^{20,21}, TGF β 1^{10,22}, Caveolin 1 (Cav1)²³, secreted frizzled-related protein (Sfrp) 1²⁴, and Phosphatase and Tensin Homolog (Pten)^{25,26}

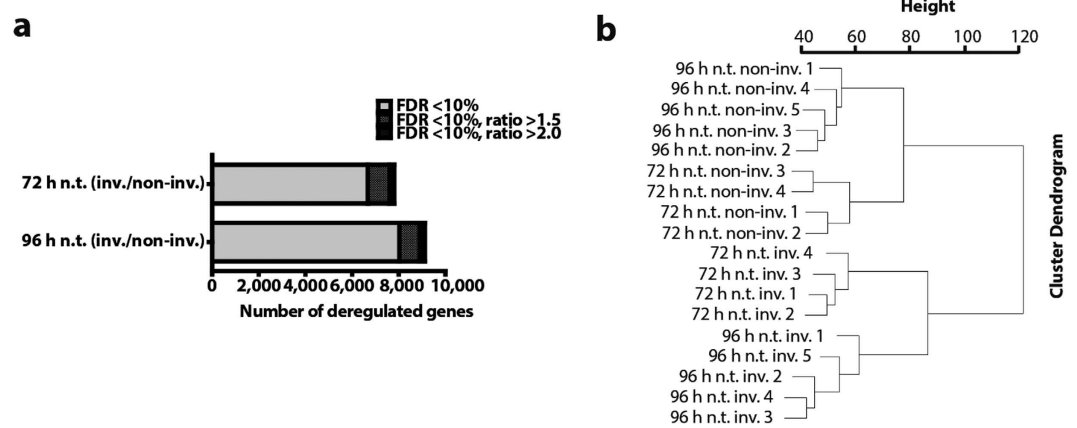


Figure 1. Analysis of differentially regulated targets of invading vs non-invading fibroblasts and hierarchical clustering. After 72 hours of invasion, 1,086 targets with expression ratios greater than 1.5-fold and 163 targets regulated greater than 2-fold were identified in the invading fraction. After 96 hours, an altered regulation of 1,049 probes with expression ratios greater than 1.5-fold and 182 greater than 2-fold were identified. The FDR for all of these targets was lower than 10%. The proportion of genes with expression ratios of $1 < < 1.5$ between invading (inv.) and non-invading (non-inv.) phenotypes are depicted in light grey. The amount of targets with an expression ratio of >1.5 and >2 is represented in dark grey and black, respectively (a). Hierarchical clustering distinguished two main clusters: invading (inv.) and non-invading (non-inv.) and two sub-clusters: 72 and 96 hours. The cluster dendrogram was conducted with R using the script hclust, on RMA data filtered for expression values >100 in at least one sample (b).

(Fig. 4A,B). Consistent with our microarray data (Fig. 4C), qRT-PCR analysis demonstrated a significant up-regulation of MMP13 and TGF β 1 in the invading fibroblasts by 6- and 1.8-fold, respectively (Fig. 4D). By contrast, Cav1, Sfrp1, and Pten were significantly down-regulated by 3.5-, 2.9-, and 2.6-fold, respectively (Fig. 3D). Reduced Sfrp1 and Cav1 protein expression was further corroborated by immunoblot analysis (Fig. 4E). Furthermore, TGF β 1 and MMP13¹⁹ were up-regulated on protein level as well (Fig. 4E). Interestingly, the protein expression of Pten, which was strongly diminished on transcript level, was found to be largely unchanged. Additionally, in primary human lung fibroblasts we identified a corresponding regulation of the same target genes in the invading subpopulation (Fig. 4F). The qRT-PCR analyses of selected target genes thus validated the robustness of our invasion assay and the identified gene signature for invading fibroblasts.

Identification and validation of upstream regulators for fibroblast invasion. In order to further validate the generated transcriptomic fibroblast invasion signature, gene expression lists were evaluated with the causal analysis tool ‘upstream regulator analysis’ (URA), implemented in IPA. This approach allowed the identification of putative upstream regulators for subsequent functional testing in regards to fibroblast invasion. In order to measure the enrichment of potentially activated upstream regulators we used a ranking based on the p-value²⁷ obtained from the overlap between our experimentally derived gene datasets and those from the IPAs database. As physiological upstream regulators were of particular interest, we excluded ‘drugs’, and ‘chemicals’ from the URA. The ‘p-value of overlap’ in supplementary Table 1 depicts a ranking of physiological upstream regulators according to their p-values for the comparison of gene expression data at 72 and 96 hours upon invasion. The cut-off value for the ranking (negative logarithmic p-value) was set to 4. By using a more stringent filter for ‘growth factors’, we were able to extract four growth factors, which all were found to be associated with fibrotic and/or cancerous diseases in the literature (Fig. 5A). Notably, TGF β 1, which is a prominent and potent activator of fibroblasts, ranked high among the predicted upstream regulators (p-value^{96 hours} = 3.2×10^{-10} , p-value^{72 hours} = 1.4×10^{-6}). In line with its key role in fibrogenesis, in the microarrays we found the expression of TGF β 1 to be significantly increased in the invading fibroblast fraction and moreover, also predicted to be associated with the generated functional gene clusters ‘IPF’, ‘invasion of cells’, and ‘metastasis’ in the *in silico* gene cluster analysis (Fig. 3C). Further putative upstream regulators from the URA, which were chosen for functional analysis in the following due to their association to fibrotic and cancerous diseases, comprised epidermal growth factor (EGF), basic fibroblast growth factor (FGF) 2, and platelet derived growth factor (PDGF)-BB. EGF, was predictively activated in the invading fibroblast fraction with a p-value^{96 hours} = 10.0×10^{-6} and a p-value^{72 hours} = 4.8×10^{-5} (Fig. 5A), while its receptor EGFR was also predicted to be activated (p-value^{96 hours} = 6.3×10^{-9} and a p-value^{72 hours} = 4.0×10^{-5}) (supplementary Table 1). In our transcriptomic invasion signature, FGF2 was another highly ranked candidate in the predicted list of upstream regulators (p-value^{96 hours} = 7.0×10^{-8} and p-value^{72 hours} = 2.8×10^{-5}), which was associated with fibrotic or cancerous diseases. Furthermore, PDGF-BB was predicted to be activated based

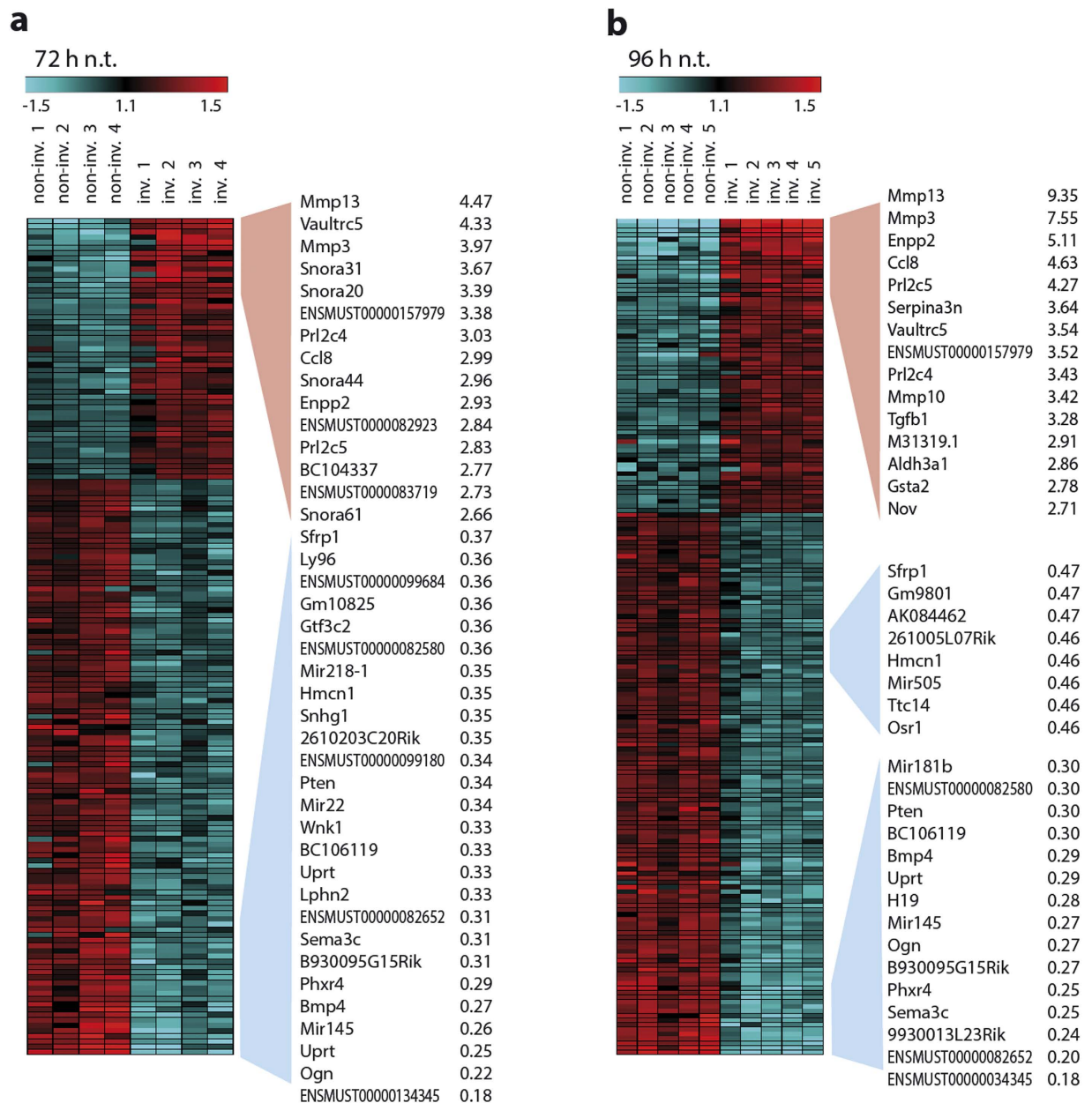


Figure 2. Transcriptome analysis (Affymetrix mouse gene ST 1.0 array) of fibroblast invasion. Separation and cell-lysis of MLg fibroblasts was performed 72 (a) and 96 hours (b) after plating the cells on top of the 3D collagen matrix. The displayed heatmaps show the top significantly up-, and down-regulated genes (>2-fold) that were found in the microarray analyses. Low and high expressed targets in the heatmap are depicted in blue and red, respectively. Each column represents one independent experiment. (n.t. = non-treated; non-inv. = non-invading fibroblasts; inv. = invading fibroblasts).

on the invasion signature with p-value $^{96\text{hours}} = 3.8 \times 10^{-6}$ and a p-value $^{72\text{hours}} = 2.3 \times 10^{-5}$. Grounded on these computational predictions of activated upstream regulators, we next performed functional confirmative studies *in vitro*. Therefore, the invasive capacity of MLg fibroblasts was assessed by using the automated software-based invasion assay recently established in our lab¹⁹. The fibroblasts were treated with the particular growth factor and the invasion capacity was measured after 72 hours total invasion time as previously described¹⁹. TGF β 1 (1 and 5 ng/ml) significantly enhanced the fibroblast invasion capacity to $138.2 \pm 28.7\%$ (p-value ≤ 0.01) and $141.7 \pm 38.1\%$ (p-value ≤ 0.01), compared to untreated controls (Fig. 5B). EGF (10 and 50 ng/ml) significantly increased the cellular invasion to $178 \pm 57.0\%$ and $193.3 \pm 64.2\%$ (p-value ≤ 0.05), respectively (Fig. 5C). FGF2 exhibited the strongest significant effect on the invasion capacity with a mean relative induction of $246.8 \pm 58.9\%$ (10 ng/ml) (p-value ≤ 0.05) and $235.0 \pm 64.2\%$ (50 ng/ml) (p-value ≤ 0.05) (Fig. 5D). PDGF-BB (5 and 25 ng/ml) initiated a significant

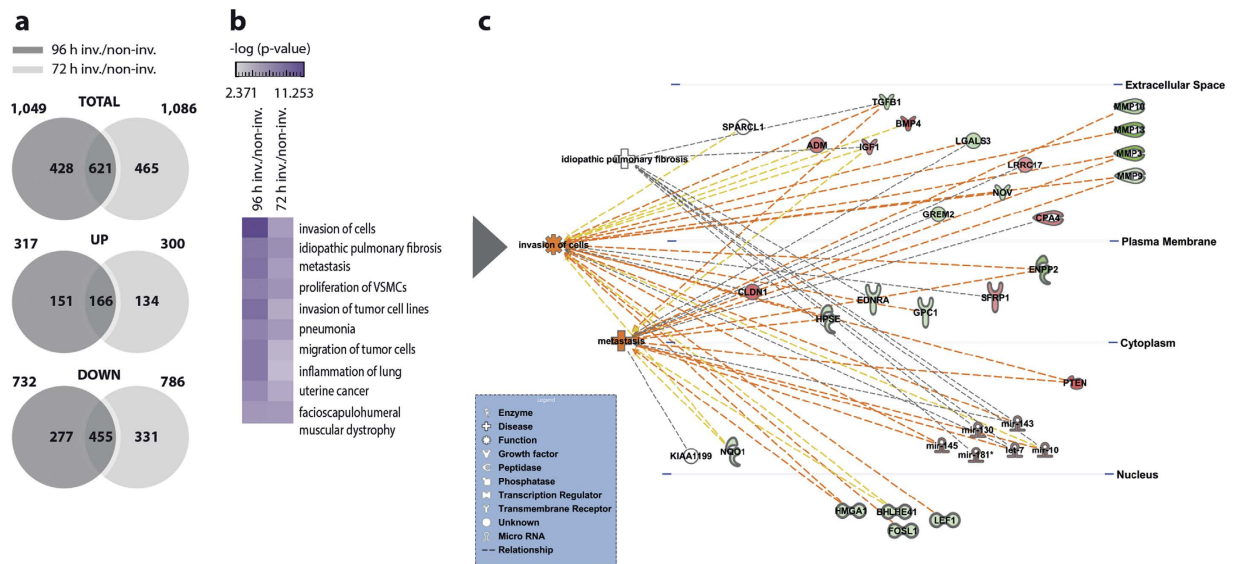


Figure 3. A time-dependent gene expression overlap of the conducted microarrays at 72 and 96 hours and predictive *in silico* analysis. Venn diagrams depict the expression overlap in deregulated genes ($>1.5x$) comparing the expression ratios of invading (inv.) and non-invading (non-inv.) fibroblasts at 96 hours and 72 hours after invasion. Note, 621 targets were found to overlap which comprise 166 up- and 455 down-regulated genes (a). An IPA generated heatmap that shows the ten most significantly over-represented ‘disease processes’ and ‘biological functions’ including ‘invasion of cells,’ ‘idiopathic pulmonary fibrosis,’ and ‘metastasis’ (b). Causal network analysis of underlying pathways of ‘invasion of cells,’ ‘idiopathic pulmonary fibrosis,’ and ‘metastasis.’ Targets that were significantly up-, or down-regulated in the invading fibroblast phenotype are represented in green and red, respectively. The dashed orange lines illustrate activating relationships, yellow lines point out findings that are inconsistent with the state of downstream molecules, and grey lines indicate that the mode of effect is not defined (c).

effect of $114.4 \pm 17.6\%$ ($p\text{-value} \leq 0.05$) and $134.9 \pm 23.0\%$ ($p\text{-value} \leq 0.001$) relative invasion (Fig. 5D). Supplementary Fig. S1 depicts representative images of either untreated or TGF β 1-, and FGF2-treated fibroblasts invading the collagen gel. Next, we used immunoblot analyses to demonstrate expression of the receptors for the above identified growth factors in lung fibroblasts. Protein expression of TGF β RI and II, EGFR, FGFR1 and 2, as well as PDGFR α and β was assessed in fibroblasts cultured on the 3D collagen matrix at the time of cell treatment. In addition, the expression levels of these receptors upon invasion were extracted from the microarray data for 72 and 96 hours of invasion (Fig. 6). While mRNA expression levels of TGF β RII and EGFR were detected but significantly reduced in invading cells at both time-points, FGFR1 and FGFR2 mRNA levels were increased. PDGFR α and β were expressed, but unchanged during invasion. Taken together, we have generated and identified, using a novel high content 3D invasion assay, a specific transcriptome signature of fibroblast invasion that shows a strong relation to invasive diseases, such as fibrosis and cancer.

Discussion

The dynamic processes of tissue remodelling and repair that take place as a physiological response to tissue injury depend on an active and versatile fibroblast phenotype that ultimately restores normal tissue architecture and homeostasis²⁸. Conversely, aberrantly activated fibroblasts are known to be involved in the initiation and progression of most malignant diseases such as cancer and fibrosis^{6,16,29}. One substantial feature of activated fibroblasts is their increased invasive capacity^{2,14}. The herein identified invasion signature included several genes that were previously reported to play essential roles for cellular invasion. In the expression profile of the invading fibroblast, the interstitial collagenase MMP13 and TGF β 1 were found to be significantly up-regulated while Cav1, Pten, and Sfrp1 were down-regulated on mRNA level. Finding MMP13 as one of the most highly up-regulated transcript in the invasion signature indicates that ECM degradation likely assists in the process of fibroblast invasion in the 3D invasion model. In a pathophysiological context, MMP13 expression in invading fibroblasts was found to not only drive their own invasion, but also influences the invasive capacity of carcinoma cells as indicated by MMP13 expression in subsets of activated carcinoma-associated fibroblasts (CAFs)^{20,30}. Up-regulation of MMP13 together with MMP1 and MMP7³¹ in lung homogenates occurs in IPF, with the main cellular source of MMP13 being the lung epithelium and interstitial spaces³². Additionally, Cav1 and Pten, which were widely studied in the context of fibrosis and cancer, as well as cellular invasion, were included in our list

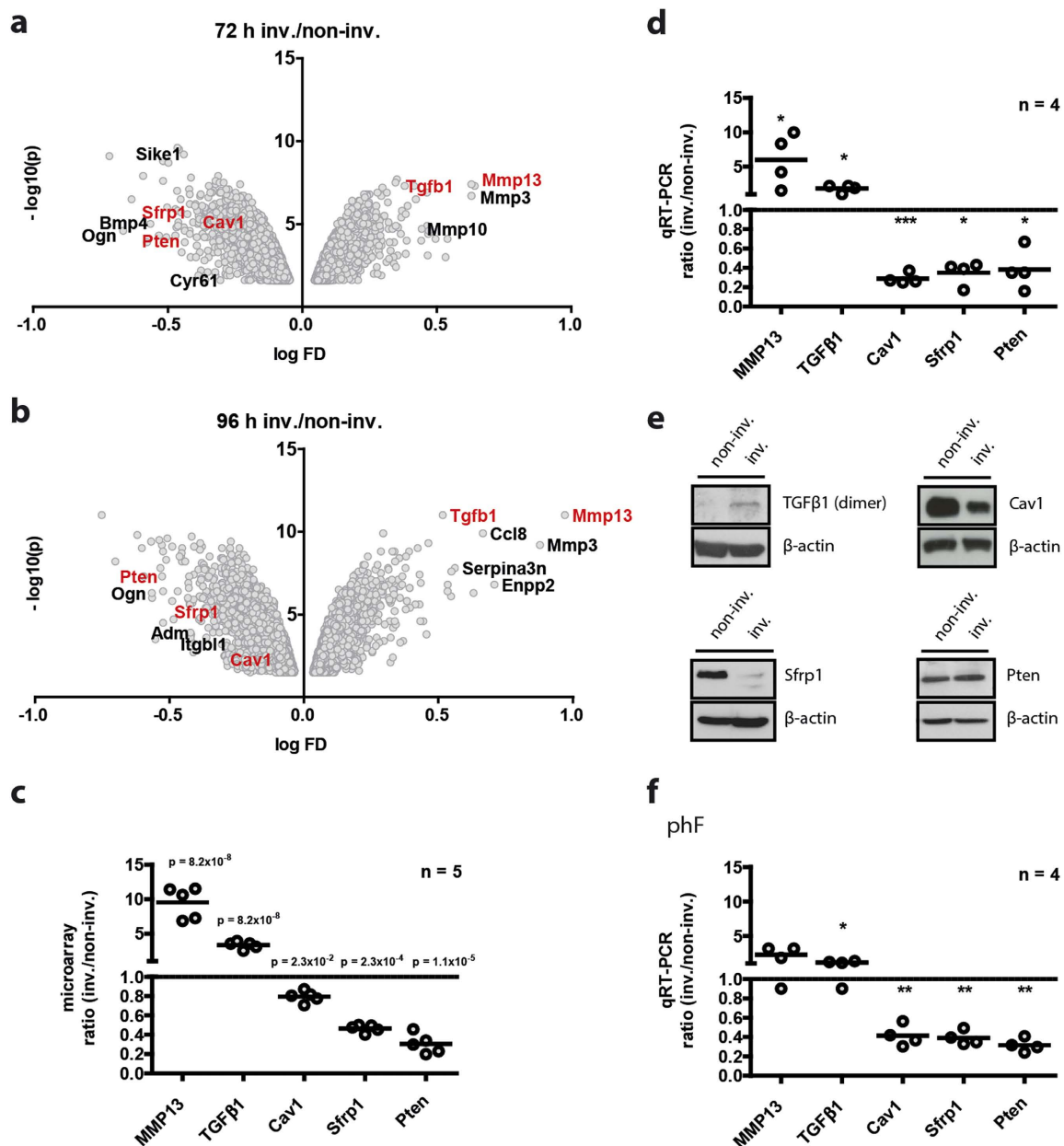


Figure 4. Expression levels of selected genes from the microarray analyses and validation by qRT-PCR and immunoblotting. Volcano plots depict the significantly differentially regulated probesets in the invading fraction at 72 (a) and 96 hours (b) time-points. Targets, used for microarray verification by qRT-PCR are highlighted in red. Here, the expression ratios derived from the microarray data are shown for a selected group of genes reportedly known to be functionally involved in the invasion of cells. The graph depicts the up-regulated targets in the invading fraction that is MMP13 (9.5x) and TGFβ1 (3.3x), as well as the down-regulated targets Cav1 (0.8x), Pten (0.3x) and Sfrp1 (0.5x) ($n = 5$). Data are shown with Benjamini-Hochberg (BH)-adjusted p-values. Genewise testing for differential expression employed the limma t-test and Benjamini-Hochberg multiple testing correction ($FDR < 10\%$) (c). qRT-PCR analyses confirming the differential expression of a selected group of genes (MMP13, TGFβ1, Cav1, and Pten) with the differential expression data derived from the microarrays. The data represent the fold induction values of the ratio between invading and non-invading fibroblasts. Data are shown as mean values from four independent experiments ($n = 4$). Statistical analysis: paired t-test. * $p < 0.05$ and *** $p < 0.001$ (d). Representative immunoblots of TGFβ1, Cav1, Sfrp1 and Pten in invading (inv.) and non-invading (non-inv.) mouse lung fibroblasts on protein level. Immunoblots were cropped to improve clarity. Uncut blots are depicted in supplementary Fig. S2 (e) in invading (inv.) and non-invading (non-inv.) mouse lung fibroblasts. qRT-PCR analyses in inv. primary human fibroblasts (phF) reveals a similar deregulation of MMP13, TGFβ1, Cav1, Sfrp1 and Pten as found in the MLg fibroblasts (f). Data shown represent mean values from four independent experiments ($n = 4$). Statistical analysis: paired t-test. * $p < 0.05$ and ** $p < 0.01$.

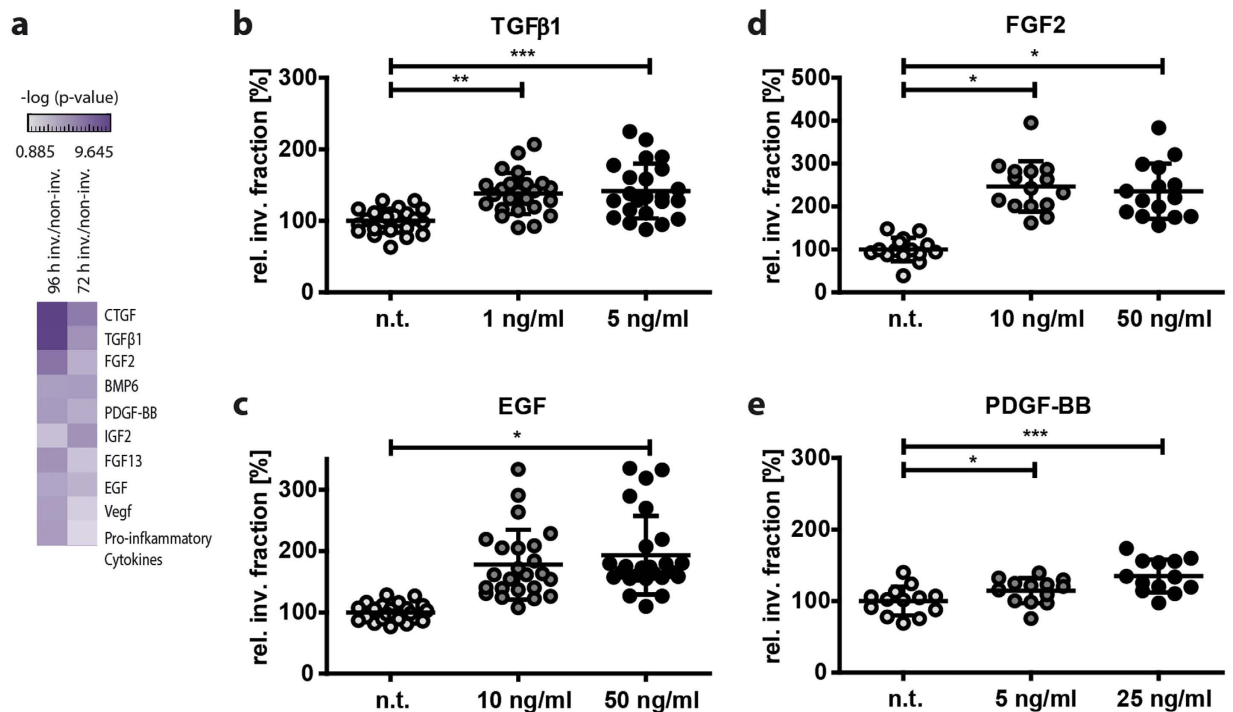


Figure 5. Causal network analysis, the identification and validation of pro-invasive growth-factors in the invasion signature of fibroblasts. A heatmap that indicates a ranking of physiological upstream regulators (filtered for ‘growth factors’) according to their p-values for gene expression data at 72 and 96 hours upon invasion (a). The predicted activated upstream regulators were functionally confirmed *in vitro* by a 3D invasion assay. Therefore, the invasive capacity of MLg fibroblasts was assessed by software-based quantification of the number of fibroblast nuclei (stained with DAPI) within and on top of the collagen matrix of 3D reconstructed confocal z-stacks. Fibroblasts were treated and left to invade the 3D collagen matrices for 48 hours. TGFβ1 (1 and 5 ng/ml), FGF2 (10 and 50 ng/ml), PDGF-BB (5 and 25 ng/ml) and EGF (10 and 50 ng/ml) were tested in the invasion assay (b–e). The data shown represent mean values (s.d.) from three to five independent experiment (n = 3–5) including five technical replicates each. (n.t. = non-treated). Statistical analysis: One way ANOVA with Dunnett’s multiple comparison test. *p < 0.05, **p < 0.01, and ***p < 0.001.

of differentially expressed targets upon invasion^{25,26,33–35}. Activated fibroblasts in IPF were reported to exhibit decreased Pten expression, correlating with increased αSMA levels³⁶. Furthermore, α5β1 integrin-mediated invasion of lung fibroblasts was found to be circumvented through the reactivation of Pten activity by α4β1 integrin²⁵. Pten also acts as stabilizer of junctional complexes in epithelial kidney cells, thereby preventing transformation to an invasive phenotype²⁶. Furthermore, Pten was reported to suppress 2D cell migration and invasion in Boyden chamber *in vitro* assays in fibroblasts^{37,38}. Interestingly, using our 3D invasion assay, protein expression of Pten did not correlate with the down-regulation of Pten on transcript level upon invasion, but remained unchanged when comparing invading with non-invading fibroblasts. This could advocate a more complex regulation of protein expression of Pten on various levels, including translation, protein stability and its turnover, or epigenetic mechanisms, all of which might be altered upon cellular invasion. Actually, the expression of Pten was reported to be regulated by miR-18a in a stiffness-dependent manner³⁹, which could influence and alter its expression levels when using soft 3D matrices, such as collagen I. In IPF, down-regulation of Pten in fibroblastic foci was found to be accompanied by decreased Caveolin 1 (Cav1) levels. Diminished Cav1 thereby reduce membrane-associated Pten, which in turn favours the activation of PI3K/Akt signal pathway⁴⁰. Furthermore, Sfrp1 was found to be down-regulated upon fibroblast invasion. Sfrps are a family of glycoproteins that can trigger Wnt signalling cascades by binding to Wnt ligands and Frizzled receptors⁴¹. Transcriptional silencing of Sfrp1 was previously reported in non-small cell lung cancer⁴² and in fibroblasts derived from keloid lesions⁴³, Systemic Sclerosis (SSc)⁴⁴, and IPF fibrotic lungs⁴⁵. In breast cancer, ectopic expression of Sfrp1 in highly invasive human derived MDA-MB-231 adenocarcinoma cells decreased the migratory potential of the cells and impaired tumour outgrowth, and blocked lung metastases²⁴. Reduction of Sfrp1 expression by TGFβ1 treatment with a concomitant increase in cell invasion and migration was reported in A549 human lung adenocarcinoma cell line⁴⁶. We also identified TGFβ1, one of the best characterized profibrotic mediators, to be up-regulated in the invasion signature⁴⁷. Here,

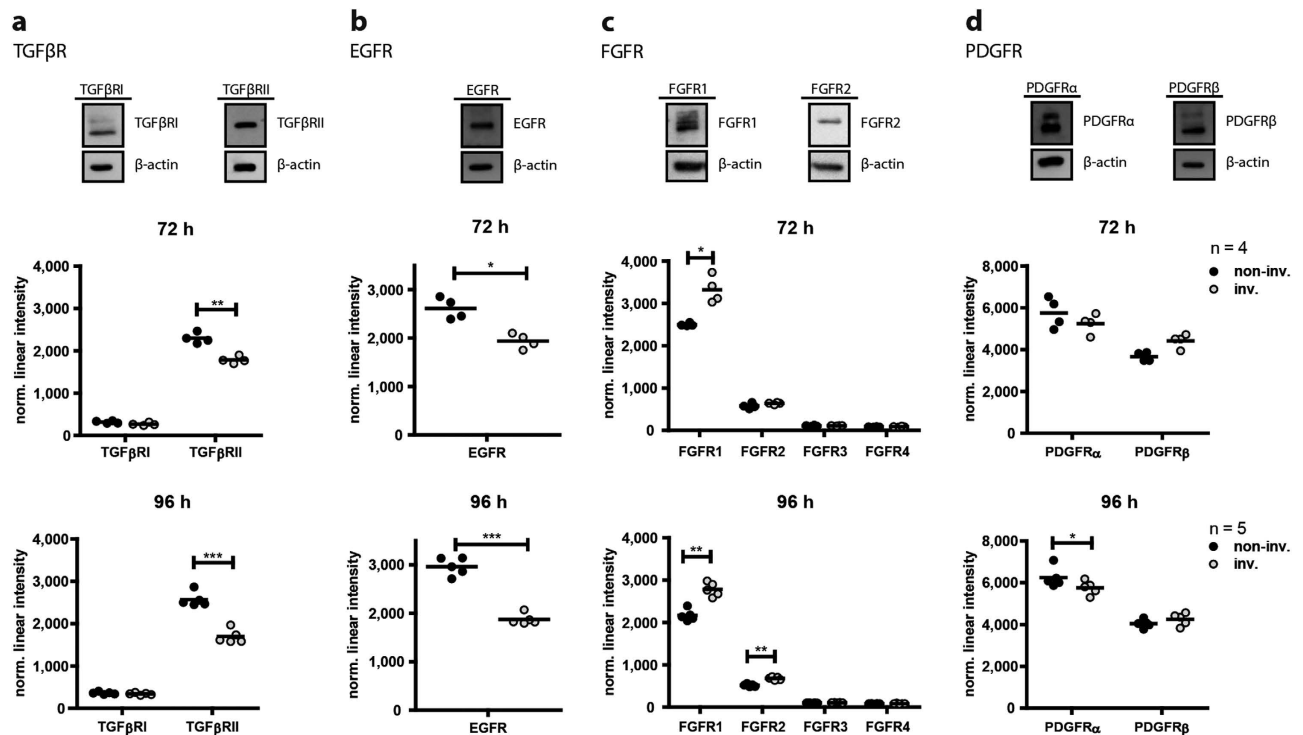


Figure 6. Expression levels of growth factor receptors. The baseline expression levels of transforming growth factor (TGF) β receptors I (TGF β RI) and II (TGF β RII), epidermal growth factor (EGF) receptor (EGFR), fibroblast growth factor (FGF) receptor 1 (FGFR1) and 2 (FGFR2), and platelet derived growth factor (PDGF) receptor alpha (PDGFR α) and beta (PDGFR β) were determined by immunoblot analysis (a–d upper panel). Expression levels upon invasion at 72 hours (72h) (a–d middle panel) and 96 hours (96h) (a–d lower panel) were extracted from the microarray data. Statistical analysis: paired t-test. * $p < 0.05$, ** $p < 0.01$, and *** $p < 0.001$.

TGF β 1 was found to be predictively associated with the functional clusters ‘invasion of cell’, ‘idiopathic pulmonary fibrosis (IPF)’, and ‘metastasis’. As the mere expression level of upstream regulators such as TGF β 1 was found to be significantly higher in invading fibroblasts, we aimed to validate the functional relevance of the generated invasion signature by using a systematic approach (Upstream Regulator Analysis (URA), Ingenuity). URA has frequently been used in the literature^{48–50}. URA enables to elucidate upstream biological causes to gene-expression datasets and thus allows interpretation of gene expression data beyond gene cluster enrichment²⁷. Using such causal networks in order to identify biological cause-effect relationships based on gene expression data is more powerful and relevant than looking at changes in gene expression levels alone²⁷. The URA of differentially expressed genes comparing invading to non-invading fibroblasts provided us with an activation list of upstream regulators of various molecule types such as cytokines, chemical drugs, kinases, transcriptional regulators, growth factors, and others. The activation of the upstream regulators is entirely based on prediction grounded on the Ingenuity Knowledge Base, which is a large collection assembled from already published findings or third-party databases. Therefore, from the list of predictively activated upstream regulators, we functionally tested several cancer- and/or fibrosis-associated growth factors in our 3D invasion assay. Consistent with the URA prediction of our experimentally derived invasion signature, TGF β 1 induced fibroblast invasion. Taking into consideration that activated, invading fibroblasts in the 3D invasion model express higher levels of TGF β 1, this invading fibroblast phenotype may initiate the activation of adjuvant fibroblasts in a pathophysiological context. Besides TGF β 1, the identification and functional verification of additional cancer or fibrosis-associated factors, EGF, FGF2 and PDGF-BB, further confirmed the functional relevance of the invasion signature. In fibrotic and cancerous diseases, epidermal growth factor (EGF) represents one potent inducer of cellular invasion, which was also shown for breast and prostate cancer cells, oral carcinoma cells⁵¹, and human dermal fibroblasts⁵². Moreover, FGF2 was reported to be highly expressed in osteosarcoma-associated stromal cells⁵³, and the expression of FGF2 was shown to be enhanced in renal fibrosis⁵⁴ as well as in bronchoalveolar lavage fluid of IPF patients⁵⁵. Furthermore, the inhibition of fibroblast growth factor receptor (FGFR) 1, the predominant receptor for FGF2, ameliorated hepatic fibrosis in a rodent model⁵⁶. Another highly ranked candidate predicted to be an activated upstream regulator in our transcriptomic invasion signature was PDGF-BB. Most recently,

PDGF-BB/PDGFR- β signalling was reported to contribute to fibrocyte migration in pulmonary fibrosis⁵⁷. In addition, an involvement of this signalling cascade was suggested for cervical cancer⁵⁸. Furthermore, it was suggested that cancer cells, secreting high amounts of PDGF activate adjuvant fibroblasts through a paracrine mechanism⁵⁹. As of now the exact mechanisms that regulate fibroblast activation and their role in the initiation and progression of diseases such as fibrosis and cancer are not fully understood. Anyway, fibroblasts might be a potent target for therapeutic intervention. As such, the transcriptomic invasion signature of fibroblasts presented in our study describes the invading phenotype to unprecedented detail and provides a powerful repository for future studies on fibroblast invasiveness and the feasibility of defining therapeutic strategies in targeting activated fibroblasts. In particular, secreted proteins such as MMP13 or Sfrp1, may represent promising therapeutic targets in pathologies exhibiting fibroblast invasion. By systematically analysing the interactome of the components identified herein, we will be able to further refine the mechanistic processes involved in fibroblast activation and invasion.

Material and Methods

Antibodies. For immunoblotting the following primary (1) and secondary antibodies (2) were used: (1) caveolin 1 (anti-cav1 (D46G3) XP, mono-clonal, rabbit, Cell Signalling (Danvers, MA, USA), 1:1,000), EGFR (anti-EGFR (D38B1), mono-clonal, rabbit, Cell Signalling, 1:1,000), FGFRI (anti-FGFRI (Ab-154), poly-clonal, rabbit, Sigma, 1:200), FGFRII (anti-FGFRII (CD332), poly-clonal, rabbit, Thermo Scientific (Rockford, IL, USA), 1:1,000), PDGFR α (anti-PDGFR α (C-20), poly-clonal, rabbit, Santa Cruz (Dallas, TX, USA), 1:500), PDGFR β (anti-PDGFR β (958), poly-clonal, rabbit, Santa Cruz, 1:1,000), Pten (138G6), mono-clonal, rabbit, Cell Signalling, 1:1,000), Sfrp1 (anti-Sfrp1 (EPR7003), mono-clonal, rabbit, Abcam (Cambridge, UK), 1:1,000), TGF β 1 (anti-TGF β 1 (ab9758), Abcam, poly-clonal, rabbit, 1:200), TGF β RI (anti-TGF β RI (H-100), poly-clonal, rabbit, Santa Cruz, 1:1,000), TGF β RII (anti-TGF β RII (D-2), mono-clonal, mouse, Santa Cruz, 1:1,000) and monoclonal mouse anti- β -Actin-Peroxidase (AC-15, Sigma, 1:10,000); (2) goat anti-rabbit and goat anti-mouse IgG conjugated to horseradish peroxidase (Cell Signalling, 1:10,000) as secondary antibody.

Cell Culture. Mouse lung fibroblasts, MLg (MLg 2908) were purchased from ATCC (Manassas, VA, USA) (CCL-206) and cultivated in DMEM/HAM's F12 (catalog# E15-813, PAA (Pasching, Austria)) medium containing 10% FBS (PAA). For isolation of primary human lung fibroblasts, specimens from lung lobes or segmental lung resections were dissected into pieces of 1–2 mm² in size and digested by 5 mg of Collagenase I (Biochrom (Berlin, Germany)) at 37°C for 2 hours. Subsequently, samples were filtered through nylon filters with a pore size of 70 μ m (BD Falcon, (Bedford, MA, USA)). Filtrates, containing the cells, were centrifuged at 400 g, 4°C for 5 minutes. Pellets were resuspended in DMEM/F-12 medium (Gibco, (Darmstadt, Germany)) supplemented with 20% fetal bovine serum (PAA) and plated on 10 cm cell-culture dishes and subsequently cultured to a confluence of 80–90% in DMEM/HAM's F12 medium containing 20% FBS. All cells were cultivated under standard conditions (5% CO₂ and 37°C). MLg fibroblasts and primary cells were not used at passage numbers higher than 15 and 10, respectively.

3D Collagen Invasion Assay. 3D cell culture assays were performed as previously described¹⁹. 2×10^4 cells per well were seeded on top of the matrix and left for invasion under standard conditions (37°C, 5% CO₂) in DMEM/HAM's F12 medium containing 5% FBS. Treatment of cells with recombinant epidermal growth factor (EGF) (Sigma), transforming growth factor beta-1 (TGF β 1) (R&D, Minneapolis, MN, USA), fibroblast growth factor (FGF) 2 (R&D) or platelet derived growth factor (PDGF) BB (life technologies; Carlsbad, USA) was accomplished by treating cells with 10–50 ng/ml EGF and FGF2, 1–5 ng/ml TGF β 1, or 5–25 ng/ml PDGF-BB 24 hours after plating, and culturing them up to 72 hours in total.

Separation Assay, Protein and mRNA Isolation from collagen-embedded Cells. The separation of invading from non-invading cells and the isolation of protein and mRNA was performed as previously described¹⁹. For immunoblot analysis of growth factor receptors, 5×10^5 cells were plated on top of 1.5 ml polymerized collagen G (Biochrom) per well of a 6-well plate in DMEM/HAM's F12 medium containing 5% FBS. Protein isolation was performed 24 hours after plating, as described before¹⁹.

mRNA Isolation and qRT-PCR. mRNA from fibroblasts, cultured in the 3D cell culture model, was isolated as previously described¹⁹. Mouse primer sequences: GTGCGAGCCGGTCATGCAGT (Sfrp1_fw), CACACGGTTGTACCTTGGGGC (Sfrp1_rev), TGTGTCCGTCGTGGATCTGA (GAPDH_fw), CC TGCTTACCACCTTCTTGA (GAPDH_rev), CGACGACGTGGTCAAGATTGACTTT (Cav1_fw), TG CACGGTACAACCGCCAG (Cav1_rev), ATCCCTTGATGCCATTACCA (MMP13_fw), AAGAGCTC AGCCTCAACCTG (MMP13_rev), GTGGACCCGAACAACGCC (TGF β 1_fw), TGGGGGTCAGCAGC CGGT (TGF β 1_rev), TCAGTGGCGGAACCTTGCAATCCT (Pten_fw), CGCCGCGTGGGTCCTGAAT (Pten_rev). Human primer sequences: GGACCGGCCATCTACCCGT (Sfrp1_fw), ACACCGTTGTGC CTTGGGGC (Sfrp1_rev), TGACCTCAACTACATGGTTTACATG (GAPDH_fw), TTGATTTTGGAG GGATCTCG (GAPDH_rev), GGACATCTTACACCGTTCCC (Cav1_fw), CTTGACCACGTCATCG TTGAG (Cav1_rev), AGGCTCCGAGAAATGCAGTC (MMP13_fw), ATCAGGAACCCCGCATCTTG (MMP13_rev), TTCGCCTTAGCGCCCACTGC (TGF β 1_fw), GGCCGGTAGTGAACCCGTTG (TGF β 1_rev), TGGCGGAACCTTGCAATCCTCAGT (Pten_fw), TCCCCTCGTGTGGGTCCTGA (Pten_rev).

cDNA was synthesized with the GeneAMP PCR kit (Applied Biosystems (Foster City, CA, USA)) utilizing random hexamers using 1 µg of isolated RNA for one reaction. Denaturation was performed in an Eppendorf Mastercycler with the following settings: lid = 45 °C, 70 °C for 10 minutes and 4 °C for 5 minutes. Reverse transcription was performed in an Eppendorf Mastercycler with the following settings: lid = 105 °C, 20 °C for 10 minutes, 42 °C for 60 minutes and 99 °C for 5 minutes. qRT-PCR reactions were performed in triplicates with SYBR Green I Master in a LightCycler® 480II (Roche (Risch, Switzerland)) with standard conditions: 95 °C for 5 min followed by 45 cycles of 95 °C for 5 s (denaturation), 59 °C for 5 s (annealing) and 72 °C for 20 s (elongation). Target genes were normalized to GAPDH expression.

Microarray. For microarray analysis, total RNA was isolated with the miRNeasy mini kit® according to the manufacturer's protocol (Qiagen (Hilden, Germany)). RNA quality was accessed by the Agilent 2100 Bioanalyzer and only high quality RNA (RIN > 8) was used for microarray analysis. Total RNA (150 ng) was amplified using the Ambion WT Expression Kit and the WT Terminal Labeling Kit (Affymetrix (Santa Clara, USA)). Amplified cDNA (2.75 µg) was hybridized on Affymetrix Mouse Gene 1.0 ST arrays containing about 28,000 probe sets. Staining (Fluidics script FS450_0007) and scanning was done according to the Affymetrix expression protocol. For the statistical transcriptome analysis, expression console (Affymetrix) was used for quality control and to obtain annotated normalized RMA gene-level data (standard settings including sketch-quantile normalisation). Array data has been submitted to GEO (GSE55322).

Protein Isolation, SDS-PAGE and Western Blotting. Protein from fibroblasts, cultured in the 3D cell culture model, was isolated as previously described¹⁹. Samples were mixed with 50 mM Tris-HCl, pH 6.8, 100 mM DTT, 2% SDS, 1% bromophenol blue, and 10% glycerol, and proteins were separated using standard SDS-10% PAGE. For immunoblotting, proteins were transferred to PVDF (Millipore (Billerica, MA, USA)), 0.45 µm or 0.2 µm membranes, which were blocked with 5% milk in TBST (0.1% Tween 20/TBS) and incubated with primary, followed by HRP-conjugated secondary antibodies over night at 4 °C and at room temperature for 1 hour, respectively.

In silico analysis. Regulated gene sets from the microarray data were analyzed through the use of IPA (Ingenuity® Systems, www.ingenuity.com). The 'disease and function' ontology was used to determine significantly enriched terms ($p > 0.01$, Right-tailed Fisher's exact test). Upstream regulator activation analysis (URA) implemented in IPA was used to predict activators that are directly or indirectly connected to the dataset of genes. Upstream regulators with a p-value of overlap ≤ 0.0001 and a positive activation z-score at both timepoints were considered activated.

Statistics. Statistical analysis was performed using GraphPad Prism4 (GraphPad Software). Data are presented as mean \pm s.d. Statistical analysis was performed using unpaired and paired t-tests (two-tailed) or One way ANOVA with Dunnett's multiple comparison test. For microarray experiments statistical analyses were performed by utilizing the statistical programming environment R implemented in CARMAweb⁶⁰. Genewise testing for differential expression was done employing limma t-test and Benjamini-Hochberg multiple testing correction (FDR < 10%). Right-tailed Fisher Exact Test was utilized for statistical analysis on the Ingenuity Pathways Analysis (IPA) platform (Ingenuity Systems (Redwood City, CA, USA)).

References

1. Lauffenburger, D. A. & Horwitz, A. F. Cell migration: a physically integrated molecular process. *Cell* **84**, 359–369 (1996).
2. Kalluri, R. & Zeisberg, M. Fibroblasts in cancer. *Nat Rev Cancer* **6**, 392–401 (2006).
3. Bhowmick, N. A., Neilson, E. G. & Moses, H. L. Stromal fibroblasts in cancer initiation and progression. *Nature* **432**, 332–337 (2004).
4. Friedl, P., Zanker, K. S. & Bocker, E. B. Cell migration strategies in 3-D extracellular matrix: differences in morphology, cell matrix interactions, and integrin function. *Microsc Res Tech* **43**, 369–378 (1998).
5. Schmidt, S. & Friedl, P. Interstitial cell migration: integrin-dependent and alternative adhesion mechanisms. *Cell Tissue Res* **339**, 83–92 (2010).
6. Klingberg, F., Hinz, B. & White, E. S. The myofibroblast matrix: implications for tissue repair and fibrosis. *J Pathol* **229**, 298–309 (2013).
7. Hardie, W. D., Glasser, S. W. & Hagood, J. S. Emerging concepts in the pathogenesis of lung fibrosis. *Am J Pathol* **175**, 3–16 (2009).
8. Cool, C. D. *et al.* Fibroblast foci are not discrete sites of lung injury or repair: the fibroblast reticulum. *Am J Respir Crit Care Med* **174**, 654–658 (2006).
9. Nasreen, N. *et al.* Pleural mesothelial cell transformation into myofibroblasts and haptotactic migration in response to TGF-beta1 *in vitro*. *Am J Physiol Lung Cell Mol Physiol* **297**, L115–L124 (2009).
10. Zolak, J. S. *et al.* Pleural mesothelial cell differentiation and invasion in fibrogenic lung injury. *Am J Pathol* **182**, 1239–1247 (2013).
11. Laurent, G. J., McAnulty, R. J., Hill, M. & Chambers, R. Escape from the matrix: multiple mechanisms for fibroblast activation in pulmonary fibrosis. *Proc Am Thorac Soc* **5**, 311–315 (2008).
12. Willis, B. C. & Borok, Z. TGF-beta-induced EMT: mechanisms and implications for fibrotic lung disease. *Am J Physiol Lung Cell Mol Physiol* **293**, L525–L534 (2007).
13. Coker, R. K. & Laurent, G. J. Pulmonary fibrosis: cytokines in the balance. *Eur Respir J* **11**, 1218–1221 (1998).

14. Li, Y. *et al.* Severe lung fibrosis requires an invasive fibroblast phenotype regulated by hyaluronan and CD44. *J Exp Med* **208**, 1459–1471 (2011).
15. Dienus, K., Bayat, A., Gilmore, B. F. & Seifert, O. Increased expression of fibroblast activation protein- α in keloid fibroblasts: implications for development of a novel treatment option. *Arch Dermatol Res* **302**, 725–731 (2010).
16. Hanahan, D. & Weinberg, R. A. Hallmarks of cancer: the next generation. *Cell* **144**, 646–674 (2011).
17. Otranto, M. *et al.* The role of the myofibroblast in tumor stroma remodeling. *Cell Adh Migr* **6**, 203–219 (2012).
18. Gaggioli, C. *et al.* Fibroblast-led collective invasion of carcinoma cells with differing roles for RhoGTPases in leading and following cells. *Nat Cell Biol* **9**, 1392–1400 (2007).
19. Burgstaller, G., Oehrle, B., Koch, I., Lindner, M. & Eickelberg, O. Multiplex profiling of cellular invasion in 3D cell culture models. *PLoS One* **8**, e63121 (2013).
20. Lederle, W. *et al.* MMP13 as a stromal mediator in controlling persistent angiogenesis in skin carcinoma. *Carcinogenesis* **31**, 1175–1184 (2010).
21. Sabeh, F., Li, X. Y., Saunders, T. L., Rowe, R. G. & Weiss, S. J. Secreted versus membrane-anchored collagenases: relative roles in fibroblast-dependent collagenolysis and invasion. *J Biol Chem* **284**, 23001–23011 (2009).
22. Imai, K. *et al.* Bronchioloalveolar invasion in non-small cell lung cancer is associated with expression of transforming growth factor- β 1. *World J Surg Oncol* **11**, 113 (2013).
23. Lino Cardenas, C. L. *et al.* miR-199a-5p is upregulated during fibrogenic response to tissue injury and mediates TGF β 1-induced lung fibroblast activation by targeting caveolin-1. *PLoS Genet* **9**, e1003291 (2013).
24. Matsuda, Y., Schlange, T., Oakeley, E. J., Boulay, A. & Hynes, N. E. WNT signaling enhances breast cancer cell motility and blockade of the WNT pathway by sFRP1 suppresses MDA-MB-231 xenograft growth. *Breast Cancer Res* **11**, R32 (2009).
25. White, E. S. *et al.* Integrin α 4 β 1 regulates migration across basement membranes by lung fibroblasts: a role for phosphatase and tensin homologue deleted on chromosome 10. *Am J Respir Crit Care Med* **168**, 436–442 (2003).
26. Kotelevets, L. *et al.* Implication of the MAGI-1b/PTEN signalosome in stabilization of adherens junctions and suppression of invasiveness. *Faseb j* **19**, 115–117 (2005).
27. Kramer, A., Green, J., Pollard, J., Jr. & Tugendreich, S. Causal analysis approaches in Ingenuity Pathway Analysis. *Bioinformatics* **30**, 523–530 (2014).
28. Hinz, B. *et al.* Recent developments in myofibroblast biology: paradigms for connective tissue remodeling. *Am J Pathol* **180**, 1340–1355 (2012).
29. Crestani, B., Besnard, V., Plantier, L., Borensztajn, K. & Mailleux, A. Fibroblasts: the missing link between fibrotic lung diseases of different etiologies? *Respir Res* **14**, 81 (2013).
30. Lecomte, J. *et al.* Bone marrow-derived myofibroblasts are the providers of pro-invasive matrix metalloproteinase 13 in primary tumor. *Neoplasia* **14**, 943–951 (2012).
31. Rosas, I. O. *et al.* MMP1 and MMP7 as potential peripheral blood biomarkers in idiopathic pulmonary fibrosis. *PLoS Med* **5**, e93 (2008).
32. Nkyimbeng, T. *et al.* Pivotal role of matrix metalloproteinase 13 in extracellular matrix turnover in idiopathic pulmonary fibrosis. *PLoS One* **8**, e73279 (2013).
33. Wang, X. M. *et al.* Caveolin-1: a critical regulator of lung fibrosis in idiopathic pulmonary fibrosis. *J Exp Med* **203**, 2895–2906 (2006).
34. Goetz, J. G. *et al.* Biomechanical remodeling of the microenvironment by stromal caveolin-1 favors tumor invasion and metastasis. *Cell* **146**, 148–163 (2011).
35. Tamura, M. *et al.* Inhibition of cell migration, spreading, and focal adhesions by tumor suppressor PTEN. *Science* **280**, 1614–1617 (1998).
36. White, E. S. *et al.* Negative regulation of myofibroblast differentiation by PTEN (Phosphatase and Tensin Homolog Deleted on chromosome 10). *Am J Respir Crit Care Med* **173**, 112–121 (2006).
37. Lilliental, J. *et al.* Genetic deletion of the Pten tumor suppressor gene promotes cell motility by activation of Rac1 and Cdc42 GTPases. *Curr Biol* **10**, 401–404 (2000).
38. Tamura, M., Gu, J., Takino, T. & Yamada, K. M. Tumor suppressor PTEN inhibition of cell invasion, migration, and growth: differential involvement of focal adhesion kinase and p130Cas. *Cancer Res* **59**, 442–449 (1999).
39. Mouw, J. K. *et al.* Tissue mechanics modulate microRNA-dependent PTEN expression to regulate malignant progression. **20**, 360–367 (2014).
40. Xia, H. *et al.* Pathologic caveolin-1 regulation of PTEN in idiopathic pulmonary fibrosis. *Am J Pathol* **176**, 2626–2637 (2010).
41. Esteve, P. & Bovolenta, P. The advantages and disadvantages of sfrp1 and sfrp2 expression in pathological events. *Tohoku J Exp Med* **221**, 11–17 (2010).
42. Fukui, T. *et al.* Transcriptional silencing of secreted frizzled related protein 1 (SFRP 1) by promoter hypermethylation in non-small-cell lung cancer. *Oncogene* **24**, 6323–6327 (2005).
43. Russell, S. B. *et al.* Epigenetically altered wound healing in keloid fibroblasts. *J Invest Dermatol* **130**, 2489–2496 (2010).
44. Dees, C. *et al.* The Wnt antagonists DKK1 and SFRP1 are downregulated by promoter hypermethylation in systemic sclerosis. *Ann Rheum Dis* **73**, 1232–1239 (2014).
45. Hsu, E. *et al.* Lung tissues in patients with systemic sclerosis have gene expression patterns unique to pulmonary fibrosis and pulmonary hypertension. *Arthritis Rheum* **63**, 783–794 (2011).
46. Ren, J. *et al.* sFRP1 inhibits epithelial-mesenchymal transition in A549 human lung adenocarcinoma cell line. *Cancer Biother Radiopharm* **28**, 565–571 (2013).
47. Fernandez, I. E. & Eickelberg, O. The impact of TGF- β on lung fibrosis: from targeting to biomarkers. *Proc Am Thorac Soc* **9**, 111–116 (2012).
48. Ampe, C., Libbrecht, J. & Van Troys, M. beta-Actin knock-out mouse embryonic fibroblasts show increased expression of LIM-, CH-, EFh-domain containing proteins with predicted common upstream regulators. *Cytoskeleton (Hoboken)* **70**, 766–774 (2013).
49. Meier-Abt, F. *et al.* Parity induces differentiation and reduces Wnt/Notch signaling ratio and proliferation potential of basal stem/progenitor cells isolated from mouse mammary epithelium. *Breast Cancer Res* **15**, R36 (2013).
50. Sachs, Z. *et al.* NRASG12V oncogene facilitates self-renewal in a murine model of acute myelogenous leukemia. *Blood* **124**, 3274–3283 (2014).
51. Lu, Z., Jiang, G., Blume-Jensen, P. & Hunter, T. Epidermal growth factor-induced tumor cell invasion and metastasis initiated by dephosphorylation and downregulation of focal adhesion kinase. *Mol Cell Biol* **21**, 4016–4031 (2001).
52. Gobin, A. S. & West, J. L. Effects of epidermal growth factor on fibroblast migration through biomimetic hydrogels. *Biotechnol Prog* **19**, 1781–1785 (2003).
53. Shimizu, T. *et al.* Fibroblast growth factor-2 is an important factor that maintains cellular immaturity and contributes to aggressiveness of osteosarcoma. *Mol Cancer Res* **10**, 454–468 (2012).
54. Strutz, F. *et al.* TGF- β 1 induces proliferation in human renal fibroblasts via induction of basic fibroblast growth factor (FGF-2). *Kidney Int* **59**, 579–592 (2001).

55. Inoue, Y., King, T. E., Jr., Tinkle, S. S., Dockstader, K. & Newman, L. S. Human mast cell basic fibroblast growth factor in pulmonary fibrotic disorders. *Am J Pathol* **149**, 2037–2054 (1996).
56. Lin, N. *et al.* NP603, a novel and potent inhibitor of FGFR1 tyrosine kinase, inhibits hepatic stellate cell proliferation and ameliorates hepatic fibrosis in rats. *Am J Physiol Cell Physiol* **301**, C469–477 (2011).
57. Aono, Y. *et al.* Role of platelet-derived growth factor/platelet-derived growth factor receptor axis in the trafficking of circulating fibrocytes in pulmonary fibrosis. *Am J Respir Cell Mol Biol* **51**, 793–801 (2014).
58. Tudoran, O. M. *et al.* PDGF beta targeting in cervical cancer cells suggest a fine-tuning of compensatory signalling pathways to sustain tumourigenic stimulation. *J Cell Mol Med* (2014).
59. Forsberg, K., Valyi-Nagy, I., Heldin, C. H., Herlyn, M. & Westermark, B. Platelet-derived growth factor (PDGF) in oncogenesis: development of a vascular connective tissue stroma in xenotransplanted human melanoma producing PDGF-BB. *Proc Natl Acad Sci U S A* **90**, 393–397 (1993).
60. Rainer, J., Sanchez-Cabo, F., Stocker, G., Sturn, A. & Trajanoski, Z. CARMAweb: comprehensive R- and bioconductor-based web service for microarray data analysis. *Nucleic Acids Res* **34**, W498–503 (2006).

Acknowledgements

The authors are grateful to Kyra Peters and Elisabeth Hennen for excellent technical assistance.

Author Contributions

B.O., designed and performed the experiments, and drafted the manuscript; G.B. designed the experiments and analyzed the data; M.I. performed the experiments and analyzed the data, S.D., J.G., T.H. performed the experiments; S.K.E., J.B., S.M. drafted the work and revised it critically for important intellectual content; O.E. designed the experiments, drafted the work and revised it critically for important intellectual content. All authors reviewed the manuscript.

Additional Information

Accession codes: GEO (GSE55322)

Supplementary information accompanies this paper at <http://www.nature.com/srep>

Competing financial interests: The authors declare no competing financial interests.

How to cite this article: Oehrle, B. *et al.* Validated prediction of pro-invasive growth factors using a transcriptome-wide invasion signature derived from a complex 3D invasion assay. *Sci. Rep.* **5**, 12673; doi: 10.1038/srep12673 (2015).



This work is licensed under a Creative Commons Attribution 4.0 International License. The images or other third party material in this article are included in the article's Creative Commons license, unless indicated otherwise in the credit line; if the material is not included under the Creative Commons license, users will need to obtain permission from the license holder to reproduce the material. To view a copy of this license, visit <http://creativecommons.org/licenses/by/4.0/>